Research Article | Vol. 28, No. 22 / 26 October 2020 / Optics Express 33682

Optics EXPRESS

Stochastic switching in the Rydberg atomic ensemble

Jun He,[1,2,3,4] Xin Wang,[1,3] Xin Wen,[1] and Junmin Wang[1,2,5]

[1] *State Key Laboratory of Quantum Optics and Quantum Optics Devices, and Institute of Opto-Electronics, Shanxi University, Tai Yuan 030006, China*
[2] *Collaborative Innovation Center of Extreme Optics of the Education Ministry and Shanxi Province, Shanxi University, Tai Yuan 030006, China*
[3] *Jun He and Xin Wang made equal contribution to this work*
[4] *hejun@sxu.edu.cn*
[5] *wwjjmm@sxu.edu.cn*

Abstract: We demonstrated stochastic switching in a bistable system implemented with the Rydberg atomic ensemble, which is realized by cascaded Rydberg excitation in a cesium vapor cell. Measurement of Rydberg state's population by means of the electromagnetically induced transparency allows us to investigate the nonlinear behavior in Rydberg atomic ensemble experimentally. The transition between the two states of the bistable system is driven by the intensity noise of the laser beams. Rydberg atomic ensemble accumulates energy in an equilibrium situation and brings the nonlinear system across the threshold, where stochastic switching occurs between the two states.

1. Introduction

System resonance is a fundamental phenomenon pervading both nature and society. It reveals the response of a system to the store and transfer of energy from an external forcing source to an internal mode, where the forcing source includes the driving signal and stochastic noise [1]. Quantum particles have been proposed as components which compose nonlinear systems. Recent developments in techniques have provided scalable approaches for studying the interplay of pure quantum mechanical systems and their couplings to reservoirs. These techniques can be applied to quantum information processing and quantum sensing [2].

The phenomena of stochastic switching in a bistable system have been observed in solid-state crystals, ion systems, and double quantum dot systems [3–10]. For atomic systems, it has been theoretically predicted that intrinsic interaction leads to stochastic resonances as well. For neutral atoms, the properties of the interaction depend on the quantum state. The interaction of the atoms in their ground state is dominated by van der Waals forces scaling as $1/R^6$ at a short range R. The excitation of the neutral atom to a high-lying Rydberg state results in strong dipole-dipole interaction or van der Waals interaction, where long-range interaction is a promising candidate for implementing a bistable system. Bistability is critical for producing stochastic switching, where quantum stochastic switching can be driven by spin noise or quantum fluctuation. Based on nonlinear systems with a cooperative Rydberg interaction, it may be possible to implement atom-based sensing. Electric sensitivity of Rydberg atoms is a promising candidate to achieve weak signal detection. The detection scheme is based on the sensitivity to the initial conditions of either stochastic or chaotic systems, in which the states of the system change under very small perturbations. This is different from the traditional methods.

We have demonstrated stochastic switching in Rydberg atomic ensemble. The double-state potential system was formed under a cooperative interaction of Rydberg atoms. In this bistable system, population transfer occurs between low and high population of Rydberg states.

#403689 https://doi.org/10.1364/OE.403689
Journal © 2020 Received 29 Jul 2020; revised 14 Oct 2020; accepted 15 Oct 2020; published 23 Oct 2020

Optics EXPRESS

2. Experimental setup

The schematic diagram of experimental apparatus is shown in Fig. 1. An 852-nm external cavity diode laser (ECDL) with a typical linewidth of ~ MHz is employed as a probe laser. The output optical power of a 1018-nm ECDL laser is amplified to 5 W by an Ytterbium-doped fiber amplifier (YDFA), and then is frequency-doubled in a PPLN crystal to produce a 509-nm laser. The two beams are then overlapped in a cesium atomic vapor cell with a counterpropagating configuration. The spherical cell has a radius of ~1.2 cm to match the Rayleigh length of the focused beams: ~ 250 µm waist for the 509-nm laser and ~170 µm waist for the 852-nm laser.

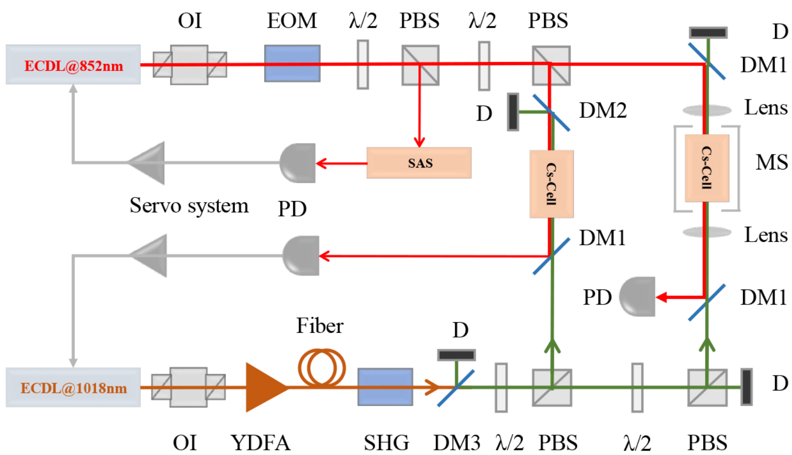

Fig. 1. Schematic of the experimental apparatus. The 852-nm external cavity diode laser (ECDL) was used as a probe laser. The 1018-nm laser from the ECDL was amplified to 5 W by the fiber amplifier, and the frequency of the output beam was doubled in a periodically poled lithium niobate (PPLN) crystal to produce a 509-nm laser (SHG). Then, the 852-nm and 509-nm laser beams overlapped in the cell (Cs-cell) in a counterpropagating configuration. OI, optical isolator; EOM, electro-optic modulator; λ/2, half-wave plate; PBS, polarization beam splitter cube; MS, Magnetic shielding; YDFA, Ytterbium-doped fiber amplifier; SHG, second-harmonic generation; PD, photodiode detector; DM1, 852-nm HR and 509-nm HT dichroic mirror; DM2, 852-nm HT and 509-nm HR dichroic mirror; DM3, 1018-nm HR and 509-nm HT dichroic mirror; D, optical dump; SAS,saturation absorption spectroscopy.

The 852-nm ECDL is stabilized to the $6S_{1/2}$ (F=4) - $6P_{3/2}$ (F'=5) hyperfine transition via the saturation absorption spectroscopy. The probe and coupling lasers' wavelengths are measured by a wavemeter (Model HighFinesse WS-7, wavelength deviation resolution is ~ 2 MHz), which is calibrated by cesium atomic hyperfine transition line. The 509-nm laser is frequency stabilized through electromagnetically induced transparency (EIT) spectroscopy. The two servo systems include piezo-electric transducer (PZT) with a kilohertz bandwidth and radio-frequency (RF) bias-Tee in current port with a gigahertz bandwidth. The bandwidth of the servo loop is over 100 kHz. The entire optical system adopts ultra-stable mirror mounts to suppress mechanical noise. The RF synthesizer (Model E-8257D, Agilent Technologies), stabilized by using a table-top rubidium atomic clock (Model FS527, SRS), is used to drive the phase-type electro-optic modulator (EOM). Based on a RF modulation technique, we have measured the velocity dependence of the hyperfine splitting of intermediate states and Doppler-free splitting of Rydberg states with the room-temperature vapor cell, as shown in Fig. 2. Measuring the energy shift by using RF modulation technique only requires frequency interval of the spectra which are clearly distinguishable.

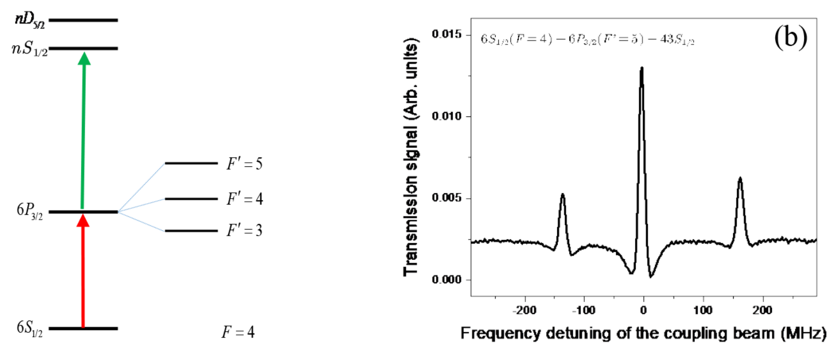

Fig. 2. (a) Energy level schematic of the cascade-type EIT of Cs atoms. The 852-nm probe laser is resonant with the $6S_{1/2}$ (F=4) - $6P_{3/2}$ (F'=5) transition. The 509-nm coupling laser is resonant with the 6P state and the nS Rydberg state. (b) All hyperfine-transition EITs of intermediate states are observed because of velocity-selective effects in the room-temperature atomic cell.

3. Cooperative Rydberg interactions

The nonlinear system produced by neutral atoms requires the preparation of a Rydberg ensemble in special quantum states.

Figure 2(a) shows cascade-type EIT of Cs atoms. The 852-nm probe laser and 509-nm coupling laser are nearly resonant. The EIT transmission signal is monitored by scanning the frequency of the coupling laser while locking the frequency of the probe laser. The strong coupling laser is scanned across the upper transition. The EIT peaks appear when the probe laser and coupling laser are two-photon resonant. The hyperfine splitting of $6P_{3/2}$ intermediate states can be observed due to the existence of different velocity classes of atoms [Fig. 2(b)]. For atoms with velocity υ moving in the same propagating direction as the probe field, the detuning of the probe laser is $\Delta_P = -\omega_P \cdot \upsilon/c$ and that of the coupling laser is $\Delta_C = \Delta_P \cdot \omega_C/\omega_P$. When the two-photon condition is satisfied, considering Doppler mismatch, the hyperfine splitting of $6P_{3/2}$ states scale as $\Delta_{Two} = -(1-\omega_C/\omega_P)\cdot\Delta_P$.

Under the weak probe field regime, the matrix element for the population can be calculated by solving the steady-state optical Bloch equations. The profile of the transmission signal amounts to a convolution of the Holtsmark probability distribution with the EIT line shape [10,11]. The evolution of the cooperative ensemble can now be described by the modified two-level optical Bloch equations [12]. Following the mean-field theory presented by Ref. [13], we simulate the Rydberg population as a function of the coupling beam's detuning, and the matrix expressions are given by

$$\dot{\rho}_{11} = \frac{i\Omega}{2}(\rho_{12}-\rho_{21}) + \Gamma\rho_{22} \tag{1}$$

$$\dot{\rho}_{12} = \frac{i\Omega}{2}(\rho_{11}-\rho_{22}) + (i\Delta_{eff} - \Gamma/2)\rho_{12} \tag{2}$$

$$\dot{\rho}_{21} = \frac{i\Omega}{2}(\rho_{22}-\rho_{11}) + (i\Delta_{eff} - \Gamma/2)\rho_{21} \tag{3}$$

$$\dot{\rho}_{22} = \frac{i\Omega}{2}(\rho_{21}-\rho_{12}) - \Gamma\rho_{22} \tag{4}$$

where Γ is the decay rate from the Rydberg state $|2\rangle$ to ground state $|1\rangle$, Ω is the Rabi frequency. The atoms in ground state are pumped to Rydberg state by probe laser and coupling laser. Here $\Delta_{eff} = \Delta - V$ is effective detuning, Δ is the detuning between the laser and transition frequencies and V is the energy shift of Rydberg atom due to the dipole-dipole interaction. The diagonal matrix elements ρ_{ii} represent the population of states and the off-diagonal matrix elements ρ_{ij} represent the coherence between the states. Following Ref. [13], the expression of population dependence is given by

$$(1-2\rho_{22})^3\left(\frac{V^2}{4}\right)+(1-2\rho_{22})^2\left(\Delta V-\frac{3V^2}{4}\right)+(1-2\rho_{22})\left(\frac{3V^2}{4}-2\Delta V+\Delta^2+\frac{\Gamma^2}{4}+\frac{\Omega^2}{2}\right)$$
$$+\left(\Delta V-\Delta^2-\frac{V^2}{4}-\frac{\Gamma^2}{4}\right)=0 \tag{5}$$

Figure 3(a) shows the population of the Rydberg state as a function of coupling laser detuning. When there is weak interaction in the Rydberg ensemble, the population varies as a function of coupling laser detuning, which is similar to a Lorentzian profile [gray dotted line in Fig. 3(a)]. When there are strong interactions, there is a sharp switching in the Rydberg population at critical laser frequency [green dash lines in Fig. 3(a)]. Here, the interaction energy is ±49 MHz, the Rabi frequency of the coupling laser and the probe laser are both 11.5 MHz. The atomic density-dependent cooperative interaction depends on the power and detuning of driving lasers. We use the EIT method to measure the population-dependent effect. The transmission signal depends on the atomic population. The simulation results are in qualitative agreement with the experimental results. The transmission spectra of the cascaded transition $6S_{1/2}$ (F=4) - $6P_{3/2}$ (F'=5) - $50D_{5/2}$ presents non-symmetric profiles as the Rabi frequency of probe laser being increased from ~3.4 MHz to ~12.5 MHz, as shown in Fig. 3(b). cooperative interaction results in the nonlinear transition effect. Here, the observed peaks shift may be also due to the ion-dependent energy shift and Cooperative interaction shift. The frequency of the probe laser is optimized by blue detuning ~200 MHz relative to the $6S_{1/2}$ (F=4) - $6P_{3/2}$ (F'=5) transition. Taking into account the Doppler mismatch, the corresponding frequency detuning of coupling laser is $\Delta_{Two} = -(1-\omega_C/\omega_P)\cdot\Delta_P \simeq -135MHz$. Note that the nonlinear collective interaction is sensitive to the ground state atomic density. The optimized temperature of the atomic gas is $35°C$, which corresponds to an atomic density of $\sim 1.3\times 10^{11} cm^{-3}$.

Figure 4 shows the dependence of the nonlinear effects on coupling laser intensity and frequency. The Rabi frequency of the coupling laser beams are increased from ~5.1 MHz to ~12.7 MHz. When the intensity of coupling beam is weak, the profile of transmission signal is similar to a Lorentzian function or a Voigt function. In the case of strong coupling beam's intensity, at critical frequency, there is a sharp switching in the transmission signal. The switching of nonlinear effect is caused by cooperative interactions in the Rydberg atomic ensemble. These interactions include the dipole–dipole interaction between Rydberg atoms [12–14], the charge-induced interaction between the Rydberg atoms and the charge produced by the spontaneous ionization of the Rydberg atoms [10,15–18]. The hysteresis phenomenon of Rydberg population depends on the laser scanning direction. The frequency of the probe laser is optimized to blue detuning of ~200 MHz relative to the $6S_{1/2}$ (F=4) - $6P_{3/2}$ (F'=5) transition. The probe laser is blue detuned by ~450 MHz relative to the $6S_{1/2}$ (F=4) - $6P_{3/2}$ (F'=4) transition, where the far-off resonance condition significantly reduces the pumping effects of Rydberg population. This may be the reason why there is no nonlinear effect for $6S_{1/2}$ (F=4) - $6P_{3/2}$ (F'=4) - $50D_{5/2}$ transition. In contrast to the power-dependent effect of probe laser, as shown in Fig. 3(b), the transmission windows of the EIT signal are not obviously shifted. The peaks shift may arise from Stark shift due to auto-ionization of the Rydberg atoms [10,18–20]. In addition, strong driving from the

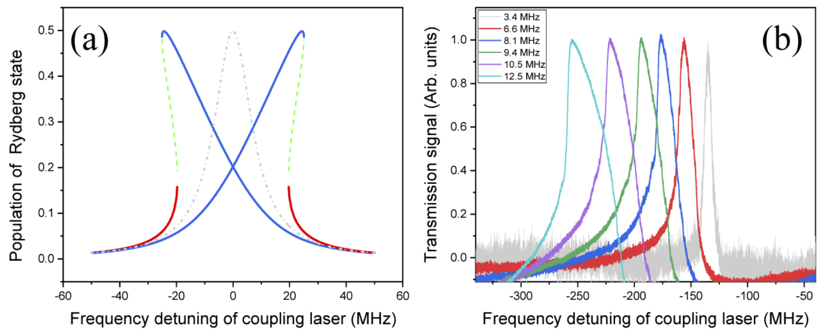

Fig. 3. (a) The population of the Rydberg state as a function of coupling laser frequency detuning. The gray dotted line is a Lorentzian profile shape. The red and blue lines plot the low and high Rydberg populations, respectively. The sign of the interaction frequency shift relative to the unperturbed resonance depends on the angular momentum states. Here, the Rabi frequency of the coupling laser and the probe laser are both 11.5 MHz. The interaction energy is ±49 MHz. (b) The transmission spectra of the cascaded transition of $6S_{1/2}$ (F=4) - $6P_{3/2}$ (F'=5) - $50D_{5/2}$ present non-symmetric profiles, the Rabi frequency of probe laser are increased from ∼3.4 MHz to ∼12.5 MHz.

probe laser inhibits the ensemble occupation of the Rydberg state, which effectively suppresses avalanche ionization, resulting in a shift in the EIT window with probe laser power [19].

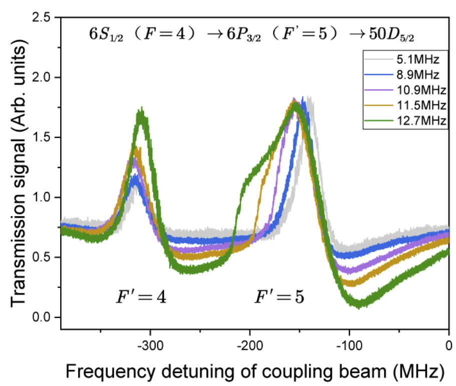

Fig. 4. Time series plots for two 6P hyperfine states with various coupling laser intensity. Distinctive nonlinear characteristics from EIT spectra are observed for the $6S_{1/2}$ (F=4) - $6P_{3/2}$ (F'=5) - $50D_{5/2}$ transition. The probe laser is optimized to blue detuning of ∼200 MHz relative to the $6S_{1/2}$ (F=4) - $6P_{3/2}$ (F'=5) transition. The Rabi frequency of the probe laser is ∼ 4 MHz.

4. Stochastic switching in a bistable system

Stochastic switching in a bistable system is similar to the threshold-crossing excitable system. The system accumulates energy in the resting state. Perturbations above a certain threshold may induce large excursions triggering transitions. When noise is injected into a bistable system, the collective interaction assists the intrinsic oscillator in eliciting an efficient response by overcoming the potential barrier. Then, the resting condition is transformed into a firing condition. The bistable system can be described by the universal scaling theory of the FitzHugh–Nagumo model [21], which is a simplified version of the Hodgkin–Huxley model [22,23]. Similarly, a Rydberg

Optics EXPRESS

atomic ensemble with long-range cooperative interaction can also perform the nonlinear system. In the case of low atomic density, the Rydberg excitations are independent, and the mutual interactions do not affect the system dynamics. As the atomic density increases, the interaction of the nearest neighbors strongly prevents the generation of new Rydberg atoms. When the number of interacting Rydberg atoms is above a critical number, the cooperative shift exceeds the width of the electron shelving resonance where the system state does not change with the laser frequency detuning in a finite range. This results in low and high Rydberg population [12,13]. The hysteresis phenomenon of Rydberg population depends on the laser scanning direction. The low and high Rydberg populations form the two stable states of system. When the driving energy is small, there is no cross motion. When the cumulative energy of the system is above the potential barrier, switching between the two states occurs.

The nonlinear interaction of the Rydberg atoms creates a two-state system. The barrier heights of the two-state can be controlled by adjusting the laser parameters. The laser beams with white Gaussian noise provide the perturbations or driving force. When the lasers derive the atomic Rydberg ensemble, the noise of laser acts on the bistable system, the cumulative energy of the system in the equilibrium state is above the barrier height, and a transition occurs between the two states of the bistable system. Figure 5(a) shows the experimental implementation of the stochastic

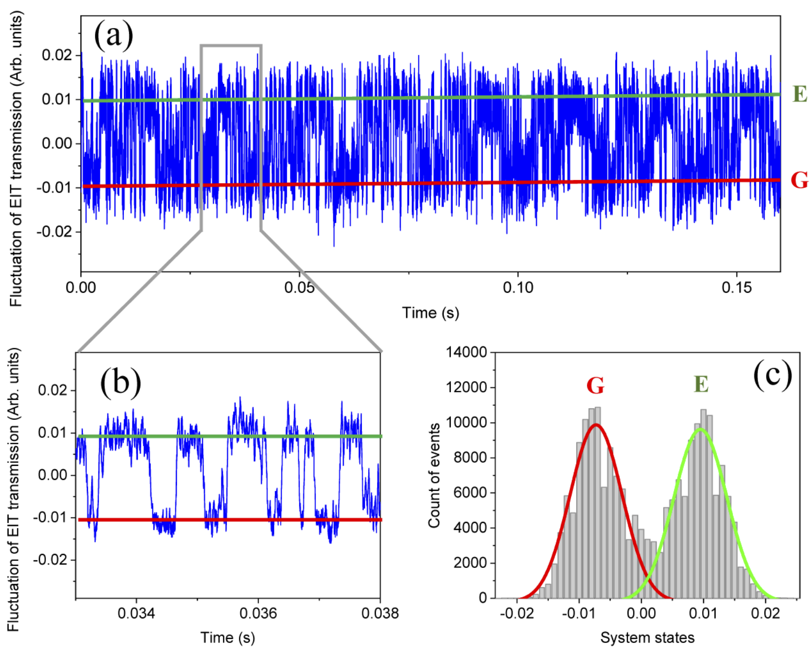

Fig. 5. Typical stochastic switching spectra: (a) Noise-induced switching traces in the nonlinear system produced by the cooperative interaction of the Rydberg atomic ensemble. G and E indicate the transmission signals for the populations of the low and high Rydberg states, respectively. For simplicity, we only show the fluctuation of EIT transmission single; (b) More detailed results, the step-like signal in detail is almost stochastic switching; (c) Histogram of the photon counting data—the discretely separated count peaks (red and green fitted lines) represent two equilibrium points in the Rydberg atomic ensemble system. Both peaks are fitted by a Gaussian function. The histogram of EIT fluctuation collected by a high-speed (Bandwidth 10 MHz) photodiode detector (Model 2015, New Focus). The voltage signal is input a digital oscilloscope (DPO7104, Tektronix), where the maximum real-time sampling rate is up to 10 GS/s. In order to reduce the signal fluctuation of discrimination, the bin size is 0.001 V.

switching for Rydberg atomic ensemble in the $50D_{5/2}$ state, as detailed in Fig. 5(b). The spectra of a time series plot are obtained by tuning the coupling laser frequency. The tolerance frequency range of stochastic switching is less than 10 MHz. The Rabi frequencies of the probe laser and the coupling laser are ~11.5 MHz and ~11.5 MHz, respectively. In the experiments, the frequency of the probe laser is blue detuned by about 200 MHz relative to the $6S_{1/2}$ (F=4) - $6P_{3/2}$ (F'=5) transition.

Almost all of the stochastic switching characteristics originate from the transition between the populations of the low and high Rydberg states. The average durations of these states are ~174 μs and ~178 μs, respectively. Typical rise and fall times are ~66 μs and ~83 μs, respectively. Figure 5(c) shows the count of events of the transmission signal. The relative occurrences number of bistability states are 49.5% and 50.5%. Clearly well-separated peaks demonstrate that there are two equilibrium points in the Rydberg atomic ensemble. The wide range of state distributions is due to system fluctuations and the conversion of the laser phase noise to amplitude noise in the EIT system. The transition characteristics are analogous to the excitation of the two-level system. The bistable system is subjected to a certain amount of internal or external random perturbations. State coherence is characterized by autocorrelations, where coherence times of ~128 μs are typical. The aperiodicity character shows that the transitions are driven by a stochastic distribution noise.

5. Summary and outlook

We explored the stochastic switching of a bistable system in the cesium Rydberg atomic ensemble. The cooperative interaction of the Rydberg atoms produces a bistable double-state system. The collective state of the Rydberg atoms accumulates energy in an equilibrium situation. External noise occasionally gives the system a kick which is large enough to cross the barrier of the double-state. Lee *et al* [24] theoretically demonstrated a collective quantum jumps of Rydberg atomic ensemble, where atomic spontaneous decay drives the stochastic jump. The quantum jump should work under the condition of cryogenic temperature to avoid the blackbody radiation. The conditions needed in experiment are difficult to be satisfied. Conservatively speaking, the cooperative interactions of the Rydberg atomic ensemble are used to establish a bistable system in our work, but the driving force of the stochastic switching may be not quantum noise. A practical case that the classical and quantum effect may be acting jointly in our experiments. An indicator of stochastic resonance is that the flow of information through a system is maximized when the input noise intensity matches the system response. This phenomenon is one of the fundamental laws in physics, engineering, biology, and etc. A quantum nonlinear system will be useful for implementing resonance sensing and precision measurements.

Funding

National Natural Science Foundation of China (61875111, 11774210, 11974226, 61905133); National Key Research and Development Program of China (2017YFA0304502); Scientific and Technological Innovation Programs of Higher Education Institutions in Shanxi Province (2017101); Fund for Shanxi Key Subjects Construction.

Disclosures

The authors declare no conflicts of interest.

References

1. S. Rajasekar and M. A. F. Sanjuan, "*Nonlinear resonances*," (Springer, 2016).
2. C. L. Degen, F. Reinhard, and P. Cappellaro, "Quantum sensing," Rev. Mod. Phys. **89**(3), 035002 (2017).
3. R. Löfstedt and S. N. Coppersmith, "Quantum stochastic resonance," Phys. Rev. Lett. **72**(13), 1947–1950 (1994).

4. V. J. Menon, N. Chanana, and Y. Singh, "Single-particle treatment of quantum stochastic resonance," Phys. A (Amsterdam, Neth.) **275**(3-4), 505–530 (2000).
5. R. L. Badzey and P. Mohanty, "Coherent signal amplification in bistable nanomechanical oscillators by stochastic resonance," Nature **437**(7061), 995–998 (2005).
6. A. Joshi and M. Xiao, "Stochastic resonance in atomic optical bistability," Phys. Rev. A **74**(1), 013817 (2006).
7. A. Joshi, "Stochastic resonance in a double quantum dot system," Phys. Rev. E **77**(2), 020104 (2008).
8. T. Wagner, P. Talkner, J. C. Bayer, E. P. Rugeramigabo, P. Hänggi, and R. J. Haug, "Quantum stochastic resonance in an ac-driven single-electron quantum dot," Nat. Phys. **15**(4), 330–334 (2019).
9. R. J. Dolleman, P. Belardinelli, S. Houri, H. S. van der Zant, F. Alijani, and P. G. Steeneken, "High-frequency stochastic switching of graphene resonators near room temperature," Nano Lett. **19**(2), 1282–1288 (2019).
10. D. Weller, J. P. Shaffer, T. Pfau, R. Löw, and H. Kübler, "Interplay between thermal Rydberg gases and plasmas," Phys. Rev. A **99**(4), 043418 (2019).
11. J. Holtsmark, "Über die verbreiterung von spektrallinien," Ann. Phys. **363**(7), 577–630 (1919).
12. C. Carr, R. Ritter, C. G. Wade, C. S. Adams, and K. J. Weatherill, "Nonequilibrium phase transition in a dilute Rydberg ensemble," Phys. Rev. Lett. **111**(11), 113901 (2013).
13. C. Carr, "Cooperative non-equilibrium dynamics in a thermal Rydberg ensemble," PhD thesis, Durham University (2013).
14. D. S. Ding, H. Busche, B. S. Shi, G. C. Guo, and C. S. Adams, "Phase diagram and self-organizing dynamics in a thermal ensemble of strongly interacting Rydberg atoms," Phys. Rev. X **10**(2), 021023 (2020).
15. N. R. de Melo, C. G. Wade, N. Šibalić, J. M. Kondo, C. S. Adams, and K. J. Weatherill, "Intrinsic optical bistability in a strongly driven Rydberg ensemble," Phys. Rev. A **93**(6), 063863 (2016).
16. D. Weller, A. Urvoy, A. Rico, R. Löw, and H. Kübler, "Charge-induced optical bistability in thermal Rydberg vapor," Phys. Rev. A **94**(6), 063820 (2016).
17. C. G. Wade, M. Marcuzzi, E. Levi, J. M. Kondo, I. Lesanovsky, C. S. Adams, and K. J. Weatherill, "A terahertz-driven non-equilibrium phase transition in a room temperature atomic vapour," Nat. Commun. **9**(1), 3567 (2018).
18. J. D. Pritchard, D. Maxwell, A. Gauguet, K. J. Weatherill, M. P. A. Jones, and C. S. Adams, "Cooperative atom-light interaction in a blockaded Rydberg ensemble," Phys. Rev. Lett. **105**(19), 193603 (2010).
19. D. Petrosyan, J. Otterbach, and M. Fleischhauer, "Electromagnetically induced transparency with Rydberg atoms," Phys. Rev. Lett. **107**(21), 213601 (2011).
20. X. Wang, J. He, J. D. Bai, and J. M. Wang, "Rydberg level shift due to the electric field generated by Rydberg atom collision induced ionization in cesium atomic ensemble," Appl. Sci. **10**(16), 5646 (2020).
21. R. FitzHugh, "Impulses and physiological states in theoretical models of nerve membrane," Biophys. J. **1**(6), 445–466 (1961).
22. J. P. Keener and J. Sneyd, "*Mathematical physiology (Vol. 1)*," (Springer, New York, 1998).
23. A. S. Mikhailov and A. Y. Loskutov, "*Foundations of synergetics II: chaos and noise*," (Springer Science & Business Media, 2013).
24. T. E. Lee, H. Häffner, and M. C. Cross, "Collective quantum jumps of Rydberg atoms," Phys. Rev. Lett. **108**(2), 023602 (2012).